

Morphology and Mechanical Properties of Fibers from Blends of a Liquid Crystalline Polymer and Poly(ethylene Terephthalate)

J. X. LI, M. S. SILVERSTEIN,* A. HILTNER,† and E. BAER

Department of Macromolecular Science and Center for Applied Polymer Research, Case Western Reserve University, Cleveland, Ohio 44106

SYNOPSIS

The domain morphology and mechanical properties of fibers spun from blends of a thermotropic liquid crystalline polymer, Vectra A-900, and poly(ethylene terephthalate) (PET) have been studied across the entire composition range. The PET phase was removed by etching to reveal fibrillar LCP domains in the blends of all compositions. The 0.5 μm fibril appeared to be the basic structural entity of the LCP domains. A primary effect of composition was the change from discontinuous fibrils when the composition was 35 and 60% by weight LCP to continuous fibrils when the composition was 85 and 96% LCP. This transition had major ramifications on the mechanical properties: the modulus increased abruptly between 60 and 85% LCP, and a change in the fracture mode from brittle fracture to a splitting mode was accompanied by an increase in fracture strength. Different models were required to describe the mechanical properties of the discontinuous and continuous fibril morphologies. Analytic models for short aligned fibers of Nielsen, and Kelly and Tyson were applicable when the LCP fibrils were discontinuous, while modulus and strength of blend fibers with continuous LCP fibrils were described by the rule of mixtures.

INTRODUCTION

The unusual rheological and mechanical properties of thermotropic liquid crystalline polymers (LCP) are well-known.^{1,2} The nematic ordered structure is responsible for the low melt viscosity and the high degree of orientation that can be achieved under elongational flow. Particularly because of the tendency for LCPs to form fibers, blends of an LCP with other thermoplastics have the potential to form in situ composites.³⁻⁵ Recent studies have described formation of fibril-like LCP domains in blends processed by conventional techniques such as extrusion, injection molding, and fiber spinning.⁶⁻⁹

This approach has certain advantages over conventional short fiber reinforcement, particularly in processing where fiber breakage, wear of the equipment, and rise of viscosity are problems typically

encountered with glass fiber reinforcement. On the contrary, addition of an LCP can actually lower the melt viscosity.¹⁰⁻¹² Furthermore, in situ formation of the fibers potentially provides a degree of control over fiber length and diameter that is not possible with glass fibers.

This work describes a study of fibers prepared from blends of an LCP with poly(ethylene terephthalate). Both polymers readily form fibers, and it was possible to prepare and characterize blend fibers over the entire composition range. The phase morphology of fibers spun from the blends was characterized, and the measured modulus and strength were compared with analytic models based on the observed morphology.

MATERIALS AND METHODS

Fibers from blends of Vectra A-900, a thermotropic liquid crystalline copolymer of hydroxybenzoic acid and hydroxynaphthoic acid (Hoechst Celanese) and poly(ethylene terephthalate) (PET) (Goodyear)

* On leave from Department of Materials Engineering, Technion, Israel Institute of Technology, Haifa, Israel.

† To whom correspondence should be addressed.

were supplied by Goodyear Tire and Rubber Company. The fibers were spun at 300°C, using a take-up speed of 85 m/min. Fibers with 96% LCP utilized a take-up speed of 403 m/min. Fibers were prepared with 0, 35, 60, 85, 96, and 100% by weight LCP; to convert the weight fraction to volume fraction, the densities of LCP and PET were taken to be 1.40 and 1.35 g/cm³, respectively.

The fibers were etched with 40% by weight aqueous methylamine solution to remove the PET. The etching solution was changed every 2 h. The etched fibers were washed with DMSO and water, then vacuum dried at room temperature. The fibers were mounted on the scanning electron microscope (SEM) stage, coated with 60–90 Å of gold, and examined in the JEOL JSM-840A scanning electron microscope.

In another experiment the fibers were completely etched without changing the etching solution. The

etching solution was centrifuged to recover dispersed LCP domains, then washed with DMSO and water. A drop of the aqueous suspension was dried on the SEM stage at room temperature, coated with gold, and examined in the SEM. The diameter and length of the LCP fibrils were measured from the SEM micrographs; the diameter, length, and aspect ratio distributions were constructed from measurements of about 500 LCP fibrils.

Fibers were fractured cryogenically by mounting a single fiber in a hand stretcher, immersing the assembly in liquid nitrogen for about a minute, and then extending the fiber rapidly until it fractured.

The tensile properties at room temperature were measured in a Minimat tensile tester (Polymer Laboratories) with a crosshead speed of 0.1 mm/min. Single fibers were adhered to a paper frame with double-sided tape and the assembly mounted in the grips of the Minimat. The two sides of the

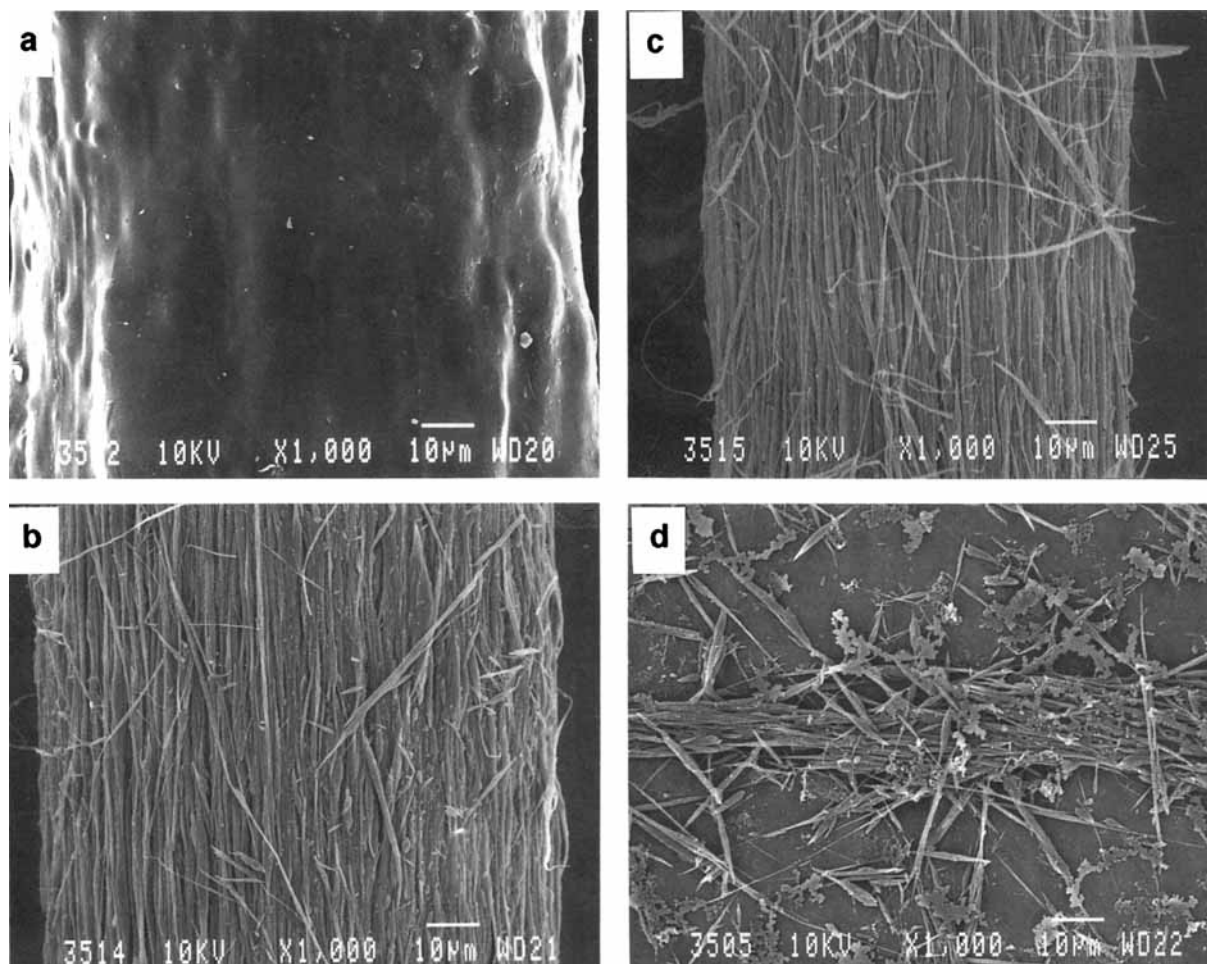


Figure 1 SEM micrographs of 35% LCP fibers. (a) Control, (b) etched for 4 h, (c) etched for 6 h, and (d) etched for 8 h.

frame were cut to leave a gauge section of fiber about 0.5 in. in length. The diameter of the fiber was measured with a micrometer and confirmed with SEM micrographs. The fiber specimen was observed during extension in the Minimat with an optical microscope. The modulus was calculated from the initial slope of the stress-strain curve and the tensile strength was taken as the stress at fracture.

RESULTS AND DISCUSSION

Fiber Morphology, Blends with 35 and 60% LCP

The surface of the as-spun 35% LCP fiber was relatively smooth [Fig. 1(a)]. Needlelike LCP fibrils, about 1 μm in diameter and aligned parallel to the fiber axis, were revealed when the fiber was etched with 40% methylamine to remove the PET [Fig. 1(b)]. The diameter of the fiber gradually decreased from about 110 μm initially to 95 μm after 4 h in the etching solution [Fig. 1(b)], and 80 μm after 6 h [Fig. 1(c)]. After 8 h, the fiber was largely disintegrated into a loose assembly of LCP fibrils; only short fragments of the original fiber, such as that shown in Figure 1(d), were found in the etching solution. After longer etching times, there was no trace of the original fiber, and the etching solution contained only a suspension of LCP fibrils.

The LCP fibrils that remained suspended in the etching solution after the PET was removed and the fiber had completely disintegrated were recovered for analysis of fibril sizes (Fig. 2). Fibril diameters were in the range of 0.5–1.5 μm . These fibrous en-

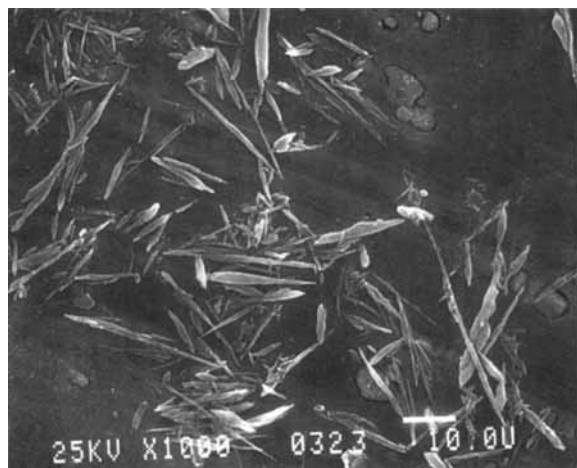


Figure 2 SEM micrograph of fibrils retrieved from the solution used to etch the entire 35% LCP fiber.

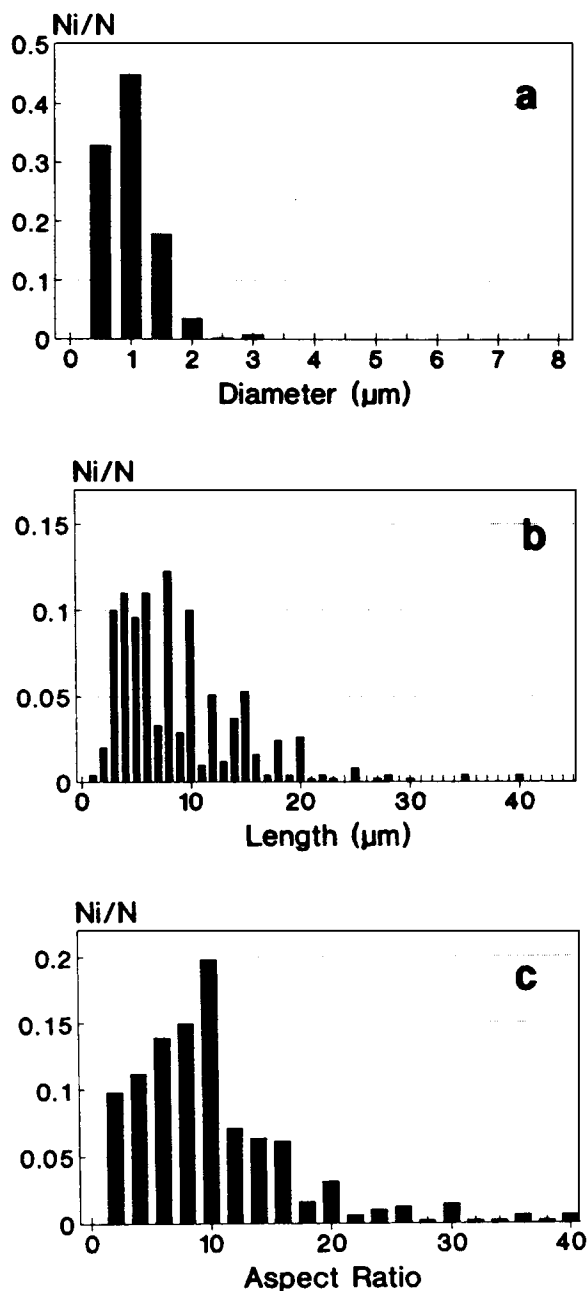


Figure 3 Distribution of LCP fibril dimensions in the 35% LCP fiber, N_i/N is the number fraction. (a) Fibril diameter distribution, (b) fibril length distribution, and (c) fibril aspect ratio distribution.

tities corresponded to one of the basic fibrillar elements in the general structural model that has been developed for highly oriented liquid crystalline fibers. The fibril is one of the basic elements of the hierarchical structural model proposed for LCP fibers, extrudates, and injection-molded articles;^{13–15} the fact that this organizational entity was observed

when the LCP was the dispersed phase of a polymer blend lent credence to the idea that this hierarchical structure is inherent to the LCP materials.

The fairly narrow distribution in fibril diameters [Fig. 3(a)], reflected the inherent tendency of the LCP to organize into fibrils at this size scale. The distribution of fibril lengths was quite broad [Fig. 3(b)]; most of the fibrils were in the range of 3–15 μm in length, but a few were as long as 40 μm . Fibril length probably depended on the amount of LCP in the blend and the flow field during processing. A result of the broad distribution in fibril lengths was a broad distribution in the aspect ratio (L/D) [Fig. 3(c)] that resembled the distribution of glass fibers created by fiber breakage during processing of reinforced composites.^{16,17} The aspect ratio ranged from 1 to 40 with a mean aspect ratio of 10. The fibril size distribution was examined at 2-h etching intervals, but no significant changes in fibril size were observed through the thickness of the fiber.

The 60% LCP fiber also had a relatively smooth surface [Fig. 4(a)], but again etching revealed LCP fibrils parallel to the fiber axis [Fig. 4(b)], although the fibrils were thicker and much longer than the LCP fibrils in the 35% LCP blend. Because the LCP fibrils were longer and more densely packed, a longer etching time was required to disintegrate the fiber into a suspension of LCP fibrils. The gradual reduction in fiber diameter that characterized etching of the 35% LCP fiber was not observed; instead, after 12 h in the etching solution, the loose assemblage of widely spaced LCP fibrils still possessed the general outline of the original fiber [Fig. 4(c)]. Only after 14.5 h when the PET was completely etched away did the fiber disintegrate into a dispersion of LCP fibrils [Fig. 4(d)].

The LCP fibrils in Figure 5(a) were taken from the etching solution used to etch the entire fiber. Closer examination of the fibrous entities in Figure 5(a) revealed that they were actually aggregates of

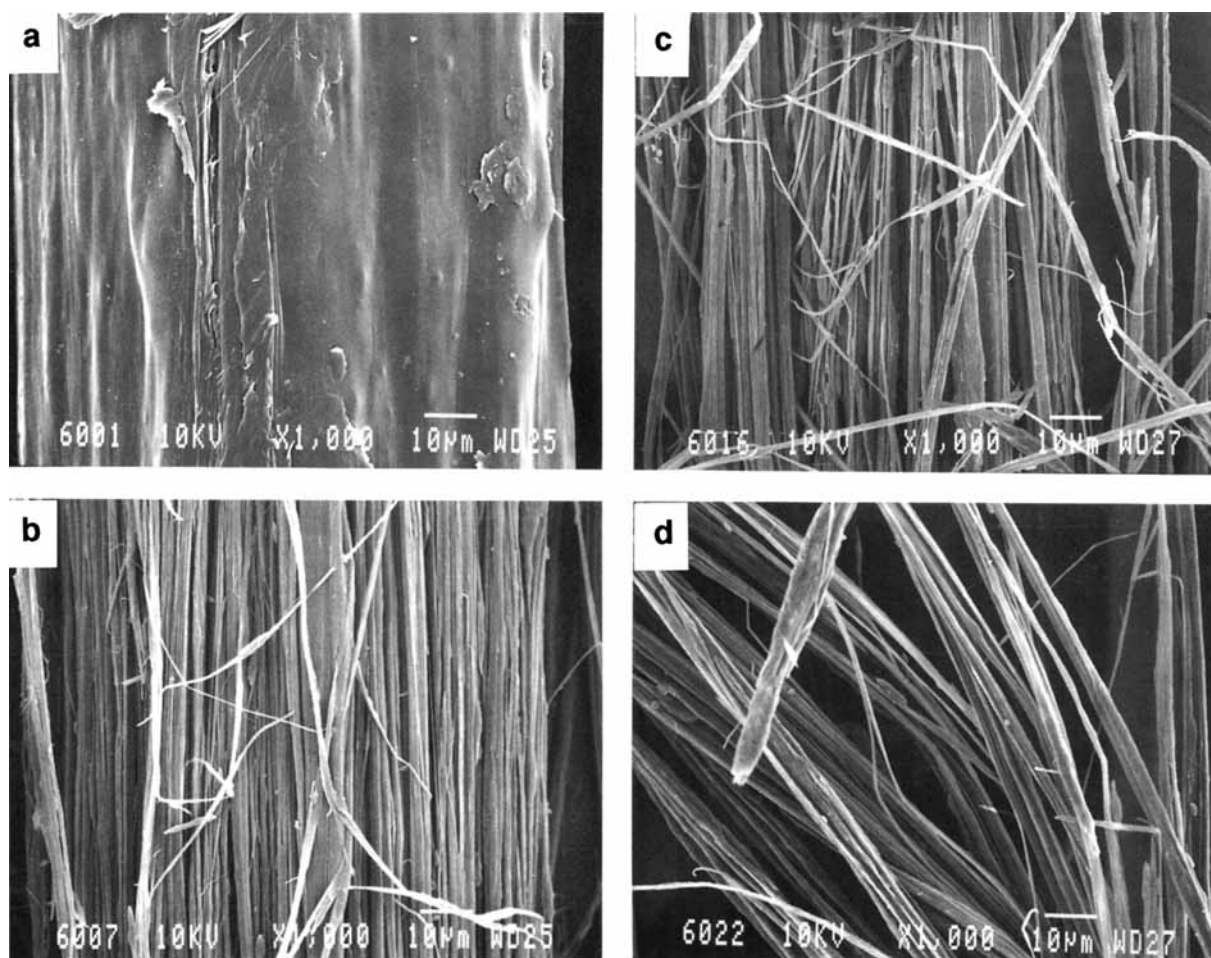


Figure 4 SEM micrographs of the 60% LCP fiber. (a) Control, (b) etched for 4 h, (c) etched for 12 h, and (d) etched for 14.5 h.

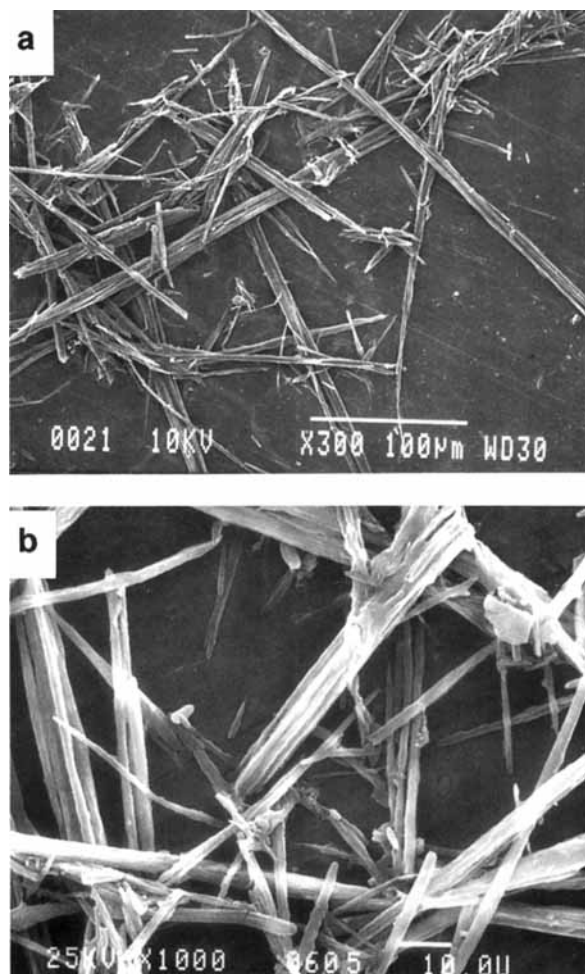


Figure 5 Fibrils retrieved from the solution used to etch the entire 60% LCP fiber. (a) Low magnification (300 \times), SEM micrograph, and (b) higher magnification (1000 \times).

1- μm fibrils [Fig. 5(b)]. A fibril of about this size is identified as a basic structural entity in the hierarchical structure of LCP fibers elucidated by Sawyer and Jaffe.^{14,15} Furthermore, these authors describe the assembly of fibrils into a larger fibrous entity, a 5- μm macrofibril. It appeared that this hierarchical structure also existed when the LCP was the dispersed phase in a blend, but the size scale to which the hierarchy developed was limited by the LCP domain size. Thus in the 35% LCP fiber, the domains consisted of LCP fibrils, while in the 60% LCP fiber the domains were assemblies of fibrils that corresponded to macrofibrils. Nevertheless, it was convenient here to refer to the LCP domains as fibrils without distinguishing the fibril and macrofibril entities.

Fibrils retrieved from the 60% LCP fiber were much thicker and also much longer than those from

the 35% LCP fiber. Comparison with the fibrils from the 35% LCP fiber (Fig. 2) emphasized the increase in length. Most of the fibril diameters were in the range of 2–5 μm , while most of the fibril lengths were in the range of 40–200 μm [Figs. 6(a) and 6(b)]. The shape of the aspect ratio distribution [Fig. 6(c)] was very similar to that of fibrils in the

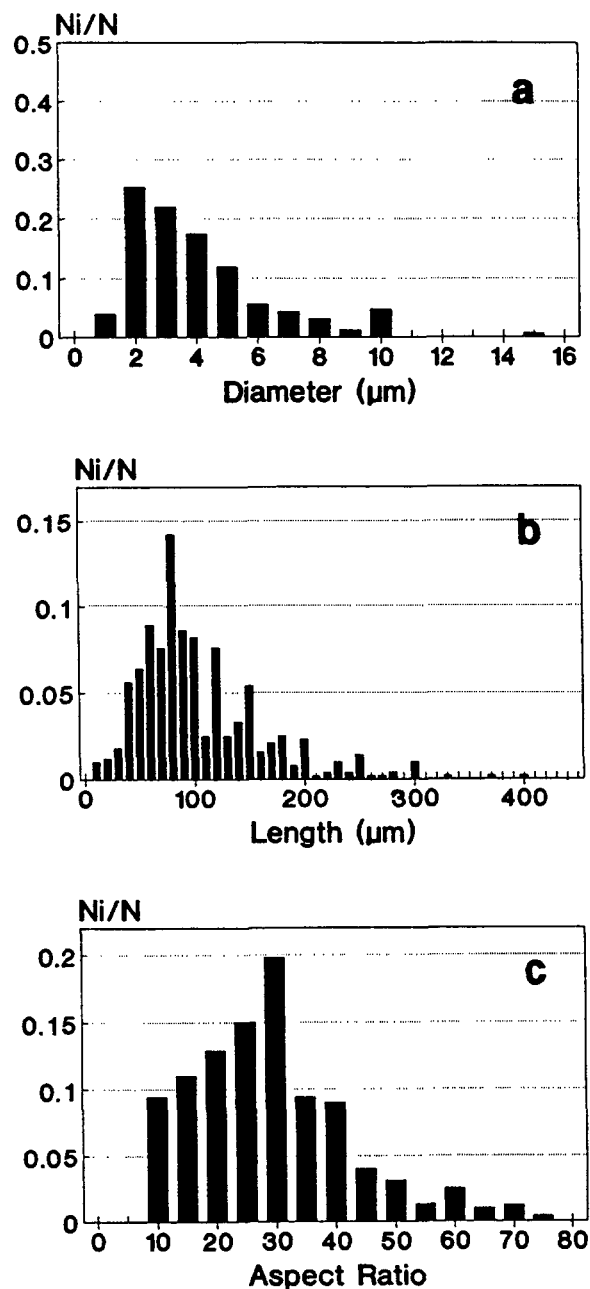


Figure 6 Distribution of LCP fibril dimensions in the 60% LCP fiber, N_i/N is the number fraction. (a) Fibril diameter distribution, (b) fibril length distribution, and (c) fibril aspect ratio distribution.

35% LCP blend. Because the fibrils were much longer in the 60% LCP fiber, the average aspect ratio was 29 compared to 10 for the 35% LCP blend, and the fibrils could be described as ranging from rodlike to fiberlike.

Fiber Morphology, Blends with 85 and 96% LCP

The fibers with higher levels of LCP, 85 and 96%, could only be etched superficially. An 85% LCP fiber showed highly oriented LCP fibrils about 0.5–3 μm in diameter after the PET skin layer was etched away [Fig. 7(a)]. Longer etching times, up to 14 h, did not lead to any further changes in the appearance of the fiber. There was no decrease in the fiber diameter during etching nor could detached LCP fibrils be recovered from the etching solution. Simi-

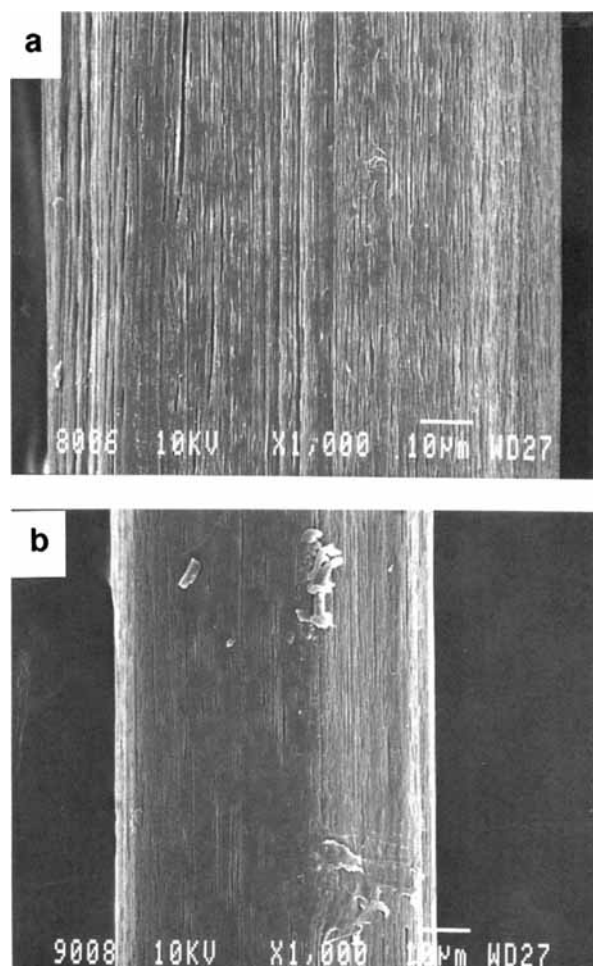


Figure 7 SEM micrographs. (a) Fiber with 85% LCP etched for 4 h and (b) fiber with 96% LCP etched for 4 h.

larly, the fiber with 96% LCP was etched only on the surface to reveal LCP fibrils 0.5–3 μm in diameter [Fig. 7(b)]. Fibril ends were rarely seen on the etched surfaces of the 85 and 96% LCP fibers, and since the etchant could not disrupt the structure, it appeared that the LCP fibrils were continuous in these compositions. The 96% LCP fibers were about 60 μm in diameter, significantly less than the 100- μm diameter of the other blend compositions. This was probably due to the higher take-up speed used during processing of this composition.

Cryogenic Fracture

The type of fracture exhibited by the fibers at cryogenic temperatures depended on the blend composition. The fibers with 35 and 60% LCP broke in a brittle manner with a sharp fracture surface. There was no evidence of damage away from the fracture site on the 35% LCP fiber [Fig. 8(a)] and only a slight amount on the 60% LCP fiber [Fig. 8(b)]. The fracture surfaces revealed protruding LCP fibrils uniformly distributed through the cross section [Figs. 8(c) and 8(d)]. The appearance of protruding fibril ends and holes created by fibril pullout on the fracture surface was consistent with the discontinuous fibril morphology of the LCP phase in these compositions. Debonding between the protruding fibrils and the PET matrix, and the clean, pulled out LCP fibrils, suggested that adhesion between the two phases was poor at cryogenic temperatures.

A second type of cryogenic fracture was exhibited by the fibers with 85 and 96% LCP, as well as the 100% LCP fiber. These fibers delaminated along the fiber axis and eventually split longitudinally during cryogenic fracture [Figs. 9(a)–9(c)]. The 0.5- μm fibrils were clearly evident when the split fibers were examined at higher magnification [Figs. 9(d)–9(f)], which suggested that interfacial failure occurred at this size scale.

Mechanical Properties

The room temperature stress–strain curves also divided the fibers into two categories (Fig. 10). The two compositions with discontinuous LCP fibrils had lower tensile moduli and tensile strengths. Examination of the fractured specimens showed that these compositions fractured perpendicular to the stress direction [Figs. 11(a) and 11(b)]. The fibers with continuous LCP fibrils had higher tensile moduli and tensile strengths and fractured by splitting

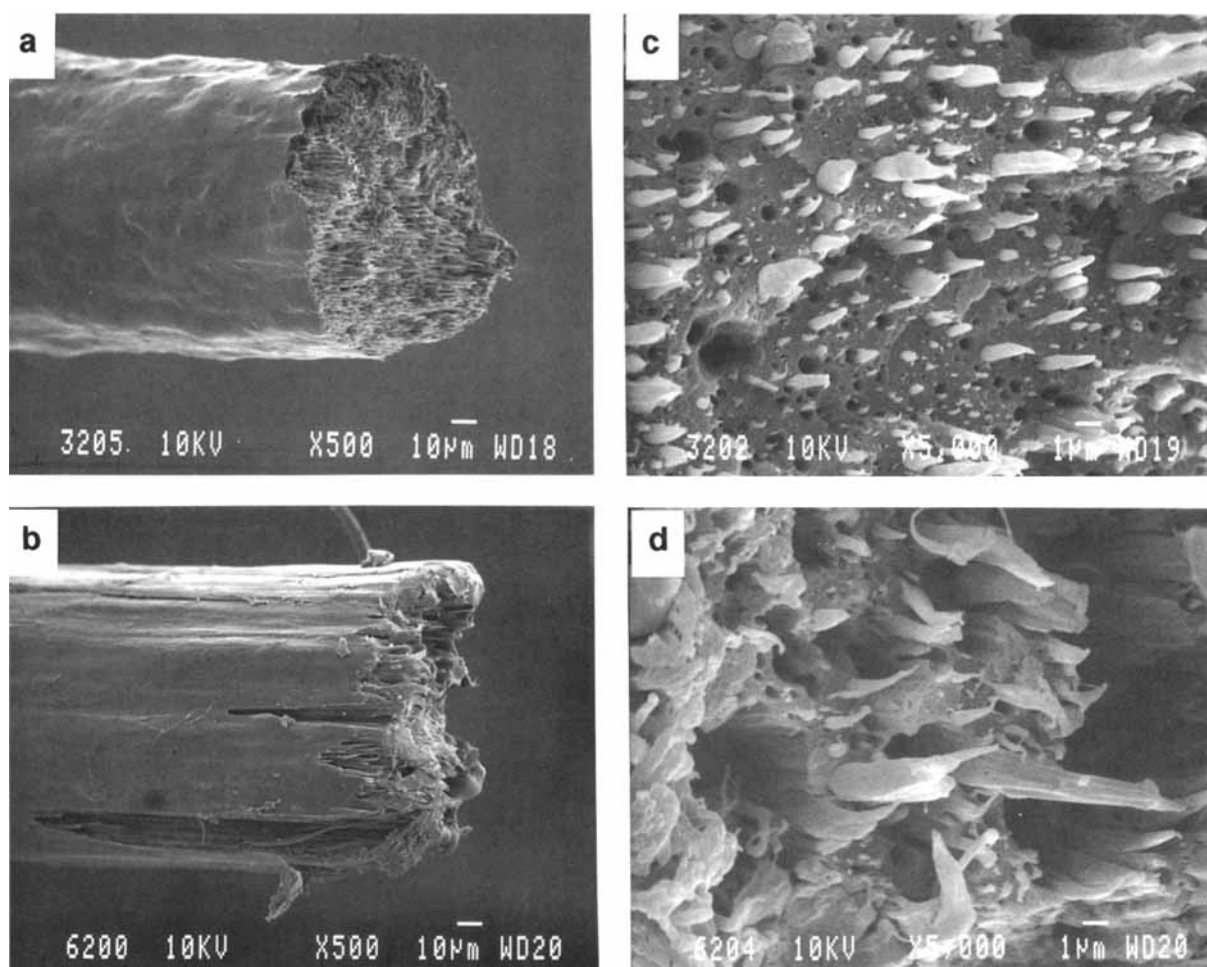


Figure 8 Cryogenic fracture surfaces. (a) The 35% LCP fiber at low magnification, (b) the 60% LCP fiber at low magnification, (c) higher magnification of (a), and (d) higher magnification of (b).

and subfibrillation [Figs. 11(c), 11(d), and 11(e)]. This latter type of fracture behavior is typical of LCPs¹³ and their blends when the LCP phase is continuous¹⁸ and provides an energy-absorbing mechanism that gives these materials unusual low temperature toughness.

Tensile Modulus

The LCP phase readily formed fibrillar domains in the blends of all compositions; the primary morphological effect of composition was the change from discontinuous fibrils when the composition was 35 and 60% LCP to continuous fibrils when the composition was 85 and 96% LCP. This transition had major ramifications on the mechanical properties: The modulus as well as the fracture mode and accompanying fracture strength changed abruptly between 60 and 85% LCP. It was apparent that the discontinuous and continuous fibril morphologies

required different models to describe the mechanical properties.

The rule of mixtures for a composite system in the linear elastic range would be the appropriate model when the higher modulus component formed a continuous phase, specifically for those blend compositions with continuous LCP fibrils, 85 and 96% LCP,

$$E_c = E_1V_1 + E_2V_2 \quad (1)$$

where E_c , E_1 , and E_2 are the moduli of the composite, PET and LCP, respectively, and V_1 and V_2 are the corresponding volume fractions obtained from the weight fractions.

The morphology of fibers with 35 and 60% LCP required a model that considered discontinuous fibers such as that of Nielsen.¹⁹ Originally developed for particulate-filled polymers, this model is also ap-

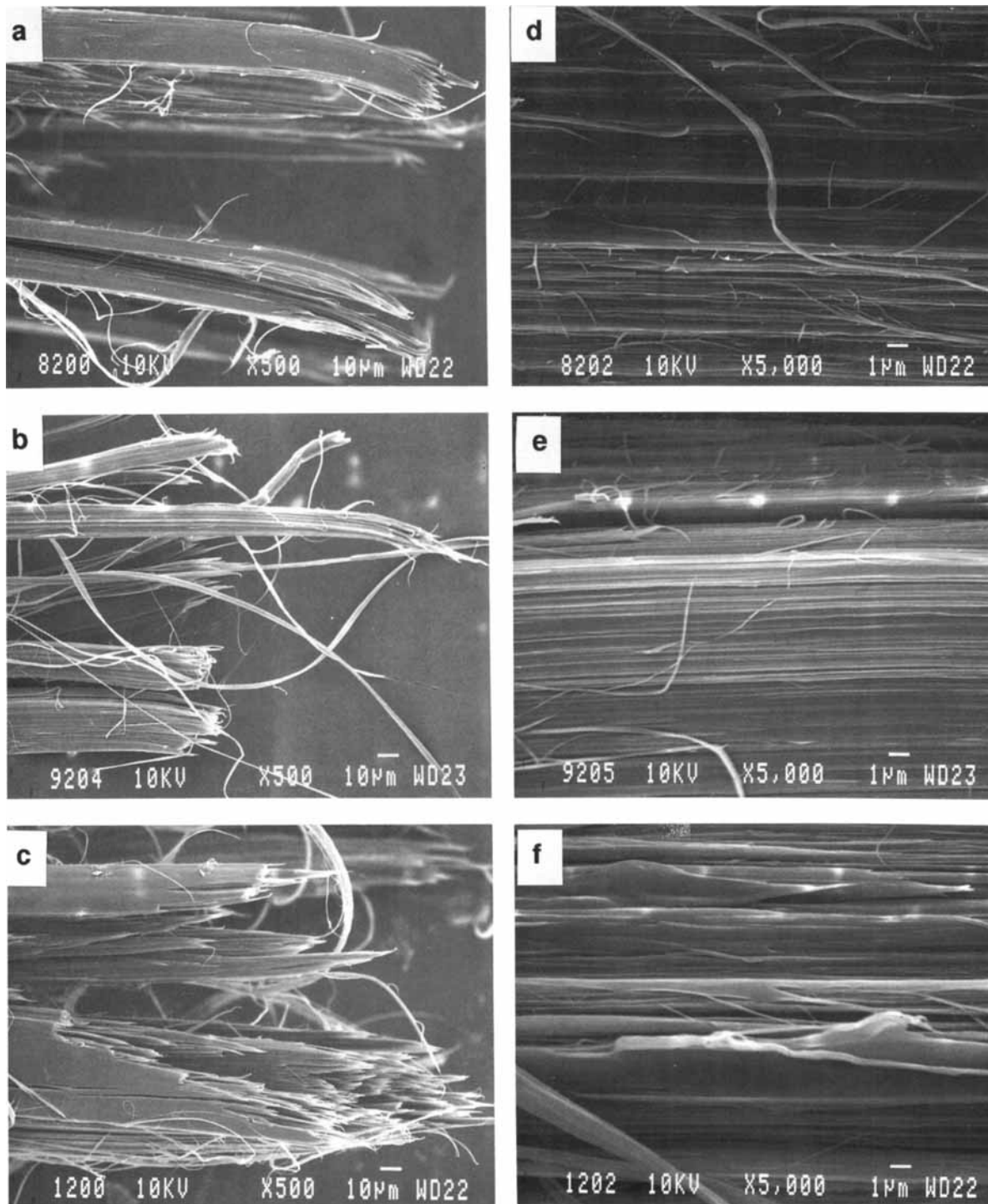


Figure 9 Cryogenic fracture surfaces. (a) The 85% LCP fiber at low magnification, (b) the 96% LCP fiber at low magnification, (c) the 100% LCP fiber at low magnification, (d) higher magnification of (a), (e) higher magnification of (b), and (f) higher magnification of (c).

plicable to other situations with short aligned fibers. This approach assumes continuity in the stress either through matrix–filler adhesion or through re-

sidual compressive stresses at the interface. Examination of room temperature fractures in the SEM showed drawn-out LCP domains with evidence

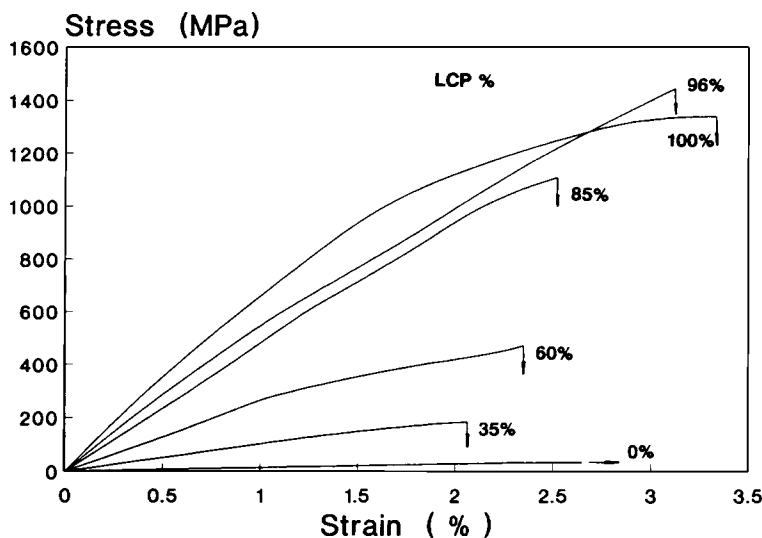


Figure 10 Stress-strain curves of fibers including the PET and LCP controls.

of good contact between the phases, which supported the assumption of stress continuity and the application of the Nielsen model to measurements made at room temperature. Use of this model was not extended to cryogenic measurements because the cryogenic fracture surfaces suggested that when fracture was carried out at low temperatures, the adhesion was poor. Possibly, good adhesion at room temperature did not persist to cryogenic temperatures because the difference in thermal expansion coefficients of the two phases caused separation at the interface.

The initial modulus is given by

$$\frac{E_c}{E_1} = \frac{1 + ABV_2}{1 - B\Psi V_2} \quad (2)$$

where

$$B = \frac{(E_2/E_1) - 1}{(E_2/E_1) + A}$$

$$\Psi = 1 + \frac{1 - \Phi_m}{(\Phi_m)^2} V_2$$

Φ_m is the maximum volume fraction that for short, perfectly aligned fibrils is 0.82¹⁹ and A is equal to twice the fibril aspect ratio (L/D) for perfectly aligned fibrils.²⁰ Since this model incorporates the aspect ratio of the fibrils, separate calculations were required for the 35 and 60% LCP fibers.

Modulus values for the two components were obtained from measurements on PET and LCP fibers. Taking the modulus of PET to be 1.5 GPa and the modulus of the LCP fibril as 70.7 GPa, the composition dependence was calculated according to

Eqs. (1) and (2) and compared with the experimentally determined moduli of the fibers (Fig. 12). The linear upper bound, obtained from the rule of mixtures [Eq. (1)], fit the experimental data for the blends with continuous LCP fibrils, 85 and 96% LCP. The observed moduli of the 35 and 60% LCP fibers were lower than predicted by the rule of mixtures. The lower two curves in Figure 12 were calculated from Eq. (2) using average values of the aspect ratio determined experimentally for these two blend compositions. The modulus of the 35% LCP fiber lay on the lowest curve, calculated for an aspect ratio of 10. Increasing the aspect ratio brought the calculated curve closer to the rule of mixtures; the measured modulus of the 60% LCP fiber lay close to the intermediate curve calculated for an aspect ratio of 29.

Tensile Strength

The expression for strength when the high-strength component, in this case the LCP, forms a continuous phase is given by

$$\sigma_c = \sigma_2 V_2 + \sigma'_1 V_1 \quad (3)$$

where σ_2 , the tensile strength of LCP, was taken from measurements on the LCP fiber to be 1.4 GPa; and σ'_1 , the stress in the PET at the strain where the fiber broke, was taken from the stress-strain curve of the PET fiber to be 45 MPa. Equation (3) was expected to apply to the 85 and 96% LCP fibers, and while the fit for the 85% LCP blend was good (Fig. 13), the strength of the 96% LCP fiber was higher than predicted, probably because the faster

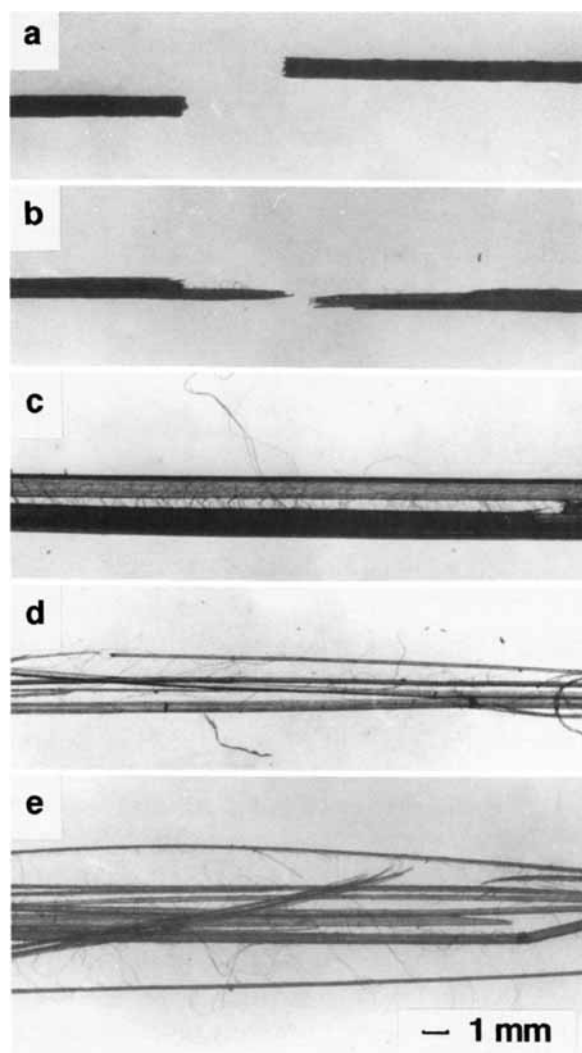


Figure 11 Fractured fibers. (a) 35% LCP, (b) 60% LCP, (c) 85% LCP, (d) 96% LCP, and (e) 100% LCP.

take-up speed used during processing gave fibers of this composition higher orientation than the others.

The strength of the 35 and 60% LCP fibers was significantly lower than calculated from Eq. (3) because the LCP fibrils were not continuous in these compositions. The Kelly and Tyson model for strength of composites with discontinuous aligned fibers was tested with these compositions.^{21,22} In the event that the aspect ratio of the fibers (L/D) is less than the critical aspect ratio, failure is assumed to occur by a pullout mechanism, and the strength depends on the interfacial shear strength τ and the tensile strength of the matrix σ_1 as follows:

$$\sigma = \left(\frac{L}{D}\right)\tau V_2 + \sigma_1 V_1 \quad (4)$$

To determine the critical aspect ratio $[L/D]_c$ of the LCP fibrils

$$\left[\frac{L}{D}\right]_c = \frac{\sigma_2}{2\tau} \quad (5)$$

it was assumed that for plastics the interfacial shear strength τ is equal to the shear strength of the matrix,²³ and for PET was estimated as $\tau = \sigma_{1y}/2$ with a value of 45 MPa used for σ_{1y} , the yield strength of PET.²⁴ In this calculation σ_2 refers to the tensile strength of the LCP fibril. Although a value of 1.4 GPa was measured for the tensile strength of the LCP fiber, it was noted that fracture occurred by splitting and subfibrillation into aggregates of fibrils, not by fracture of individual fibrils. Presumably, then, the strength of individual fibrils is greater than 1.4 GPa. The fibril strength must be at least as high as the strength attained with the highly oriented commercial LCP fiber, 3 GPa.²⁵ Further justification for the use of this value for the strength was the fact that the commercial fibers have a diameter of 10–20 μm , similar to that of the LCP fibrils, and therefore fracture would have occurred on a similar size scale. Using this value for σ_2 , the critical aspect ratio calculated from Eq. (5) was 67. This meant that fibrils in both 35 and 60% LCP fibers were below the critical aspect ratio and Eq. (4) was appropriate for these compositions.

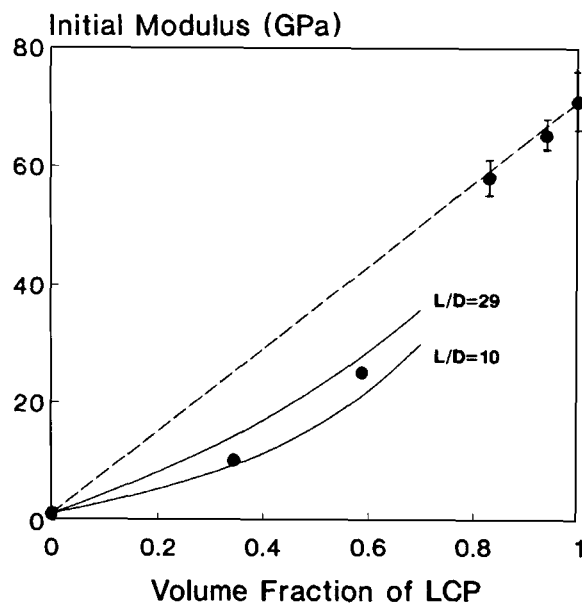


Figure 12 Comparison of calculated and observed modulus. ● Experimental data, --- rule of mixtures [Eq. (1)], and — short aligned fibers [Eq. (2)].

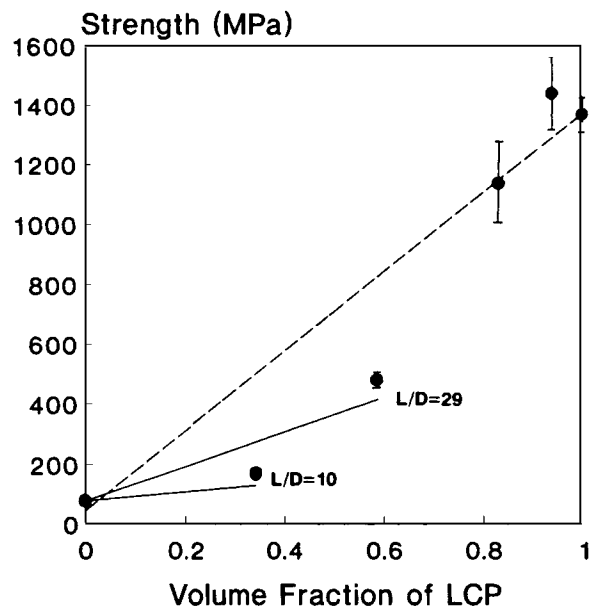


Figure 13 Comparison of calculated and observed strength. ● Experimental data, --- continuous fibers [Eq. (3)], and — discontinuous fibers [Eq. (4)].

The average L/D values measured from the micrographs were used in Eq. (4) with a value of 78 MPa for σ_1 measured from a PET fiber to obtain the lower curves in Figure 13. The experimental points lie close to the calculated curves, the strength of the 60% LCP fiber is close to that calculated for an aspect ratio of 29 and the strength of the 35% LCP fiber close to that for an aspect ratio of 10. Further evidence that the LCP fibers were below the critical aspect ratio and Eq. (4) was appropriate for these compositions came from the fracture surfaces where there was no evidence of fiber fracture, instead, fracture occurred with interfacial failure followed by fiber pullout as the model required.

CONCLUSIONS

This study of the relationships between the morphology of fibers spun from blends of a thermotropic liquid crystalline polymer and PET and the mechanical properties in tension has led to the following conclusions:

1. Discontinuous fibrous LCP domains were found in the fibers with 35 and 60% by weight LCP. When the LCP content was higher, 85 and 96%, the fibrous LCP phase was contin-

uous. The basic structural entity of the LCP domains was the 0.5- μm fibril.

2. The transition from discontinuous to continuous LCP fibrils was accompanied by an increase in modulus and strength with a change in the fracture mode from brittle fracture when the LCP fibrils were discontinuous to delamination fracture when the LCP was continuous.
3. Analytic models for short aligned fibers were applicable when the LCP fibrils were discontinuous, while modulus and strength of fibers with continuous LCP fibrils were described by the rule of mixtures.

Sincere thanks are due to Dr. Harlan W. Frerking and Ms. Judy Tweedie of The Goodyear Tire and Rubber Company who provided samples and the fiber etching method. This research was generously supported by The Goodyear Tire and Rubber Company and the Army Research Office, grant number DAAL03-88K-0097.

REFERENCES

1. A. Ciferri, W. R. Krigbaum, and R. B. Meyer, Eds., *Polymer Liquid Crystals*, Academic, New York, 1982.
2. M. G. Dobb and J. E. McIntyre, in *Advances in Polymer Science*, Vol. 60/61, Springer-Verlag, Berlin, 1984.
3. G. Kiss, *Polym. Eng. Sci.*, **27**, 410 (1987).
4. R. A. Weiss, W. Huh, and L. Nicolais, *Polym. Eng. Sci.*, **27**, 684 (1987).
5. B. R. Bassett and A. F. Yee, *Polym. Compos.*, **11**, 10 (1990).
6. A. I. Isayev and M. Modic, *Polym. Compos.*, **8**, 158 (1987).
7. C. U. Ko and G. L. Wilkes, *J. Appl. Polym. Sci.*, **37**, 3063 (1989).
8. A. M. Sukhadia, D. Done, and D. G. Baird, *Polym. Eng. Sci.*, **30**, 519 (1990).
9. G. Crevecoeur and G. Groeninckx, *Polym. Eng. Sci.*, **30**, 532 (1990).
10. A. Siegmann, D. Dagan, and S. Kenig, *Polymer*, **26**, 1325 (1985).
11. K. G. Blizard and D. G. Baird, *Polym. Sci. Eng.*, **27**, 653 (1987).
12. A. Kohli, N. Chung, and R. A. Weiss, *Polym. Eng. Sci.*, **29**, 573 (1989).
13. T. Weng, A. Hiltner, and E. Baer, *J. Mater. Sci.*, **21**, 744 (1986).
14. L. C. Sawyer and M. Jaffe, *J. Mater. Sci.*, **21**, 1897 (1986).
15. L. C. Sawyer and M. Jaffe, in E. Baer and A. Moet, Eds., *High Performance Polymers*, Hanser, Munich, 1991.

16. H. Voss and K. Friedrich, *J. Mater. Sci.*, **21**, 2889 (1986).
17. C. Kau, A. Hiltner, and E. Baer, *J. Reinforc. Plast. Compos.*, **8**, 18 (1989).
18. M. S. Silverstein, A. Hiltner, and E. Baer, *J. Appl. Polym. Sci.*, **43**, 157 (1991).
19. L. E. Nielsen, *Mechanical Properties of Polymers and Composites*, Vol. 2, Marcel Dekker, New York, 1981, Chapter 7.
20. L. E. Nielsen, *Mechanical Properties of Polymers and Composites*, Vol. 2, Marcel Dekker, New York, 1981, Chapter 8.
21. D. Hull, *An Introduction to Composite Materials*, Cambridge University Press, 1981, Chapter 9.
22. J. K. Lees, *Polym. Eng. Sci.*, **8**, 195 (1968).
23. R. Nicholls, *Composite Construction Materials Handbook*, Prentice-Hall, Englewood Cliffs, NJ, 1976, Chapter 11.
24. D. L. Wilfong, A. Hiltner, and E. Baer, *J. Mater. Sci.*, **21**, 2014 (1986).
25. Data supplied by Hoechst-Celanese Research Co., Summit, NJ 07901.

Received April 30, 1991

Accepted May 17, 1991